analytical chemistry

pubs.acs.org/ac
Article

Synthetic Protein-to-DNA Input Exchange for Protease Activity Detection Using CRISPR-Cas12a

Luca Capelli,[§] Federica Pedrini,[§] Andrea C. Di Pede, Alejandro Chamorro-Garcia, Neda Bagheri, Simone Fortunati, Marco Giannetto, Monica Mattarozzi, Roberto Corradini, Alessandro Porchetta, and Alessandro Bertucci*

Cite This: *Anal. Chem.* 2024, 96, 18645−18654

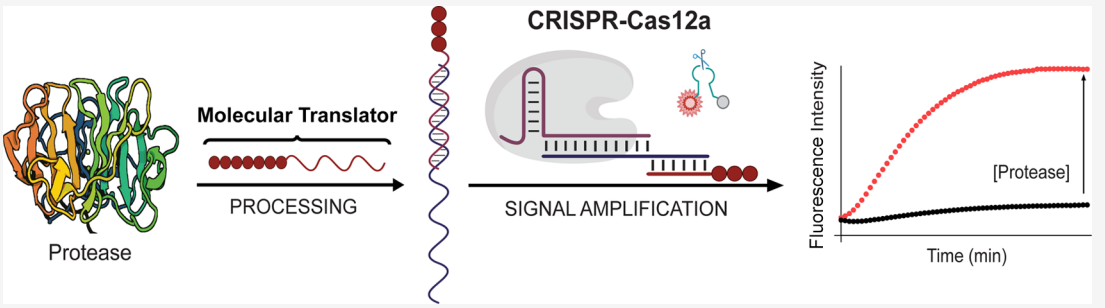

ABSTRACT: We present a novel activity-based detection strategy for matrix metalloproteinase 2 (MMP2), a critical cancer protease biomarker, leveraging a mechanism responsive to the proteolytic activity of MMP2 and its integration with CRISPR-Cas12a-assisted signal amplification. We designed a chemical translator comprising two functional units—a peptide and a peptide nucleic acid (PNA), fused together. The peptide presents the substrate of MMP2, while the PNA serves as a nucleic acid output for subsequent processing. This chemical translator was immobilized on micrometer magnetic beads as a physical support for an activity-based assay. We incorporated into our design a single-stranded DNA partially hybridized with the PNA sequence and bearing a region complementary to the RNA guide of CRISPR-Cas12a. The target-induced nuclease activity of Cas12a results in the degradation of FRET-labeled DNA reporters and amplified fluorescence signal, enabling the detection of MMP2 in the low picomolar range, showing a limit of detection of 72 pg/mL. This study provides new design principles for a broader applicability of CRISPR-Cas-based biosensing.

INTRODUCTION

Activity-based diagnostics are emerging sensing technologies that leverage the enzymatic activity of a protein to generate measurable outputs.[1] Unlike conventional immunoassays, these diagnostics offer unique advantages, including direct measurement of enzyme activity, specific substrate recognition, and real-time monitoring.[2,3] Beyond merely indicating the presence of a target protein, activity-based diagnostics can provide insights into its active biological state.[4] One specific area of interest for activity-based sensing is the detection and quantification of human proteases, a crucial class of hydrolytic enzymes responsible for degrading proteins, activating zymogens, and regulating numerous biological processes.[5−7] Among these, matrix metalloproteinases (MMPs), a family of zinc-dependent proteases capable of degrading extracellular matrix components, have garnered significant attention due to their potential as drug targets and biomarkers for cancer diagnosis.[8−10] In cancer, MMPs play a critical role in promoting invasion and metastasis, and their dysregulated expression profile serves as a distinctive trait of different tumors.[11−13] The activity-based quantification of specific MMPs can be achieved using fluorogenic peptide substrates. Typically, these peptides are labeled with a fluorophore/quencher pair, and a fluorescence signal is generated upon MMP-mediated hydrolytic cleavage.[14] Various classes of probes for this purpose are commercially available. However, these exhibit certain limitations, such as relatively high background signals and an inability to manipulate the output signal or integrate with signal amplification processes, which limits their sensitivity.[15,16] To address these challenges and enhance sensitivity, activity-based mechanisms have been combined with various optical and electrochemical assays, often leveraging nanomaterials to obtain amplification of the

Received: May 20, 2024
Revised: August 26, 2024
Accepted: September 6, 2024
Published: November 14, 2024

https://doi.org/10.1021/acs.analchem.4c02622
Anal. Chem. 2024, 96, 18645−18654

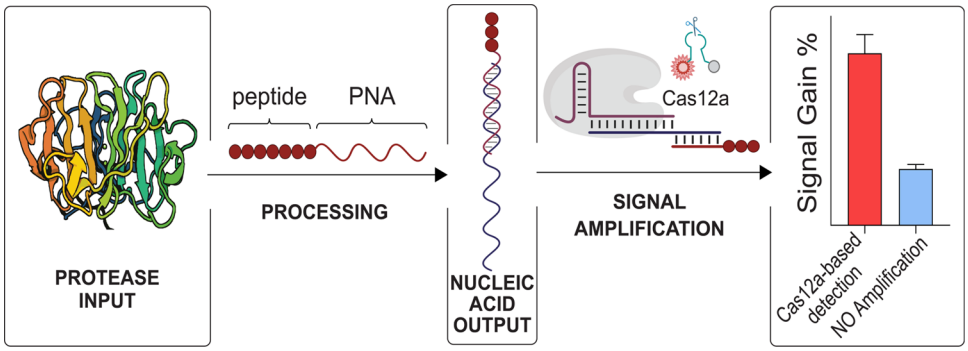

Figure 1. Schematic illustration of the proposed MMP2 activity-based detection method, leveraging a synthetic protein-to-DNA input exchange. A peptide-PNA chemical translator is used to convert MMP2 enzymatic activity into an input for CRISPR-Cas12a-based signal amplification.

output signal.[17−23] Recently, innovative approaches involving nucleic acid-based amplification processes have emerged, which hold promise for advancing activity-based protein detection through DNA nanotechnology.[24−26] These include strategies that leverage protease-triggered activation of an inactive T7 RNA polymerase and subsequent signal amplification based on the transcription of functional RNA sequences.[27,28] One exceptionally powerful tool in nucleic acid diagnostics is signal amplification based on programmable single-stranded DNA (ssDNA) aspecific cleavage by preactivated CRISPR-Cas12a.[29−32] When the collateral cleavage of CRISPR-Cas12a is activated in the presence of FRET-labeled DNA reporters, substantial signal amplification can be obtained, enabling ultrasensitive detection of the nucleic acid target.[33] To date, only a limited number of CRISPR-Cas-based sensing methods have been reported for the detection of targets such as proteins and small molecules, as this necessitates the development of nontrivial strategies for converting a non-nucleic acid target into a nucleic acid-based input for CRISPR-Cas activation.[29,34,35] Bhathia and coworkers have recently demonstrated that CRISPR-Cas12a can be used to read and amplify urinary biomarkers for multiplexed and portable cancer diagnostics. These synthetic urine biomarkers are constructed using a nanocarrier functionalized with chemically stabilized DNA-barcoded protease-responsive peptides, allowing for *in vivo* sensing of proteolytic activity in murine cancer models.[36] Kang et al. engineered anti-CRISPR proteins to create CRISPR-Cas protein switches for viral protease detection, showing conversion of specific proteolytic events into the activation of Cas12a function with high switching ratios.[37] While this paper was under review, Pandit et al. reported DNA-barcoded plasmonic nanostructures enabling CRISPR-Cas12a-based amplification of protease activity. These probes are composed of gold nanoparticles functionalized with peptide−DNA conjugates. The peptide is the substrate of the protease of interest, and the DNA serves as a barcode that identifies the peptide. Following proteolytic cleavage, this DNA sequence can be measured via a CRISPR/Cas12a-based assay, enabling detection of the SARS-CoV-2-associated protease, 3CL, and the apoptosis marker, caspase 3, with an LOD of 59 pM.[38] The primary objective of our study was to explore a novel and straightforward avenue for integrating CRISPR-Cas12a amplification into a protease activity-based assay, thereby introducing a new modality for the nucleic acid-based processing of protein inputs. We specifically focused on MMP2, a critical protease biomarker that has a fundamental role in various types of cancer, where its dysregulated expression is implicated in tumor advancement, invasion, metastasis, and angiogenesis.[39−42] To achieve the conversion of MMP2 enzymatic activity into a synthetic nucleic acid-based input for CRISPR-Cas12a, we designed a chemical translator that incorporates a peptide and a peptide nucleic acid (PNA) unit. The peptide unit presents the sequence specifically processed by MMP2, while the PNA unit facilitates the conversion of peptide cleavage into nucleic acid output. This translator was anchored to magnetic microbeads (MBs), which serve as physical supports in the design of the activity-based assay. Hybridized with the PNA unit is a specific ssDNA sequence carrying a free region complementary to the CRISPR RNA (crRNA) of the CRISPR-Cas12a system. This ssDNA serves as an activator of CRISPR-Cas12a. Upon MMP2 enzymatic cleavage, the nucleic acid portion (composed by a shortened peptide-PNA conjugate and by the DNA partially hybridized to it) is released, and the free DNA single strand segment can activate CRISPR-Cas12a, initiating the degradation of rationally designed hairpin DNA reporters labeled with a fluorophore/quencher pair. This process generates an amplified fluorescence signal enabling the quantification of MMP2 in the low picomolar range (Figure 1).

EXPERIMENTAL SECTION

Synthesis of the Peptide-PNA Chemical Translator. The synthesis of the peptide-PNA conjugates utilized as chemical translators was performed with standard manual Fmoc-based solid-phase synthesis using HBTU/DIPEA as coupling mixture and commercially available Fmoc-AA−OH monomers (Sigma-Aldrich, Merck KGaA, Darmstadt, Germany) and Fmoc-PNA−OH monomers (Biosearch Technologies, Bellshill, Scotland), following established protocols. Rinkamide-ChemMatrix resin was first loaded with Fmoc-$Lys_{(Dde)}$−OH as the first monomer (0.13 mmol/g). Two versions of peptide-PNA translators that differ in the presence of a fluorescent tag were prepared. Both of the translators have the same peptide-PNA sequences (reported below), with an azide group at the N-end. The azide group was introduced by reacting the translator with preactivated azidoacetic acid, using HBTU/DIPEA as an activating mixture. Prior to cleavage from the resin, the Dde (2-Acetyldimedone) protecting group on the side chain of the lysine residue was removed with a solution of *N*-methyl-2-pyrrolidone, hydroxylamine, and imidazole in DMF. In the case of the peptide-PNA translator labeled with a fluorescent tag, the side chain of the lysine was used as an anchor point for a TAMRA molecule, which was introduced by reacting preactivated (through HBTU/DIPEA

https://doi.org/10.1021/acs.analchem.4c02622
Anal. Chem. 2024, 96, 18645−18654

mixture) 5(6)-carboxy-tetramethylrhodamine with the amino group on the translator. Cleavage from the resin was performed with a solution of 10% m-cresol in trifluoroacetic acid (TFA). The purification of the above peptide-PNA conjugates was performed by RP-HPLC (Agilent 1260 Infinity) with UV detection at λ 260 nm using a semi-preparative C_{18} column (5 μm, 250 × 10 mm, Jupiter Phenomenex, 300 Å), eluting with H_2O containing 0.1% TFA (eluent A) and CH_3CN containing 0.1% TFA (eluent B); elution gradient: from 100% A to 50% B over 30 min, flow rate: 4 mL min^{-1}. The purity and identity of the purified peptide-PNA conjugates were determined by HPLC−ESI/MS (Dionex Ultimate 3000 equipped with linear ion trap detector) using a Phenomenex Gemini C_{18} column: 100 mm × 4.6 mm, 3 μm.

Analysis of MMP2-Mediated Proteolytic Cleavage of the Peptide-PNA Translator. A solution of peptide-PNA chemical translator (0.5 μM) in TRIS containing $CaCl_2$ 0.1 mM was incubated with MMP2 at a 1:0.1 ratio for 24 h at 37 °C. The analyses were conducted using a Dionex Ultimate 3000 High-Performance Liquid Chromatography (HPLC) system (Thermo Scientific) coupled to an Orbitrap LTQ XL mass spectrometer (Thermo Scientific). Chromatographic separation was achieved using a Kinetex C18 column (Phenomenex, 50 mm × 2.1 mm, 2.6 μm, 100 Å). The instrument operated via gradient elution with a mobile phase composed of Phase A (0.1% formic acid v/v in water) and Phase B (0.1% formic acid v/v in acetonitrile); elution gradient: from 99% A to 95% B over 40 min. The mobile phase flow rate and injection volume were set at 200 μL/min and 5 μL, respectively, with an acquisition delay of 3.50 min.

Melting Measurement. Melting curves were recorded by heating 1 mL of an equimolar solution (5 μL) of peptide-PNA translator and DNA activator and following the UV signal variation at 260 nm. Melting temperatures were taken as the maximum of the first derivative of the melting curve. The UV data were recorded on a Thermo Scientific Evolution 260 Bio UV−visible spectrophotometer.

Functionalization of Magnetic Beads with the Peptide-PNA Translator. Aminated magnetic beads (0.1 mg/mL) were initially washed with pure DMSO, then resuspended in a 2.5 mM solution of DBCO-NHS in DMSO with DIPEA added, and incubated for 2 h at 25 °C under constant shaking (1500 rpm). After that, the beads were washed with DMSO to remove unreacted DBCO-NHS and incubated with a fresh solution of azide-modified peptide-PNA translator in TRIS buffer (0.1 mg/mL) for 3.5 h at 37 °C. Eventually, the beads were washed three times with distilled water.

Characterization of the Functionalization Steps. ATR-FT-IR measurements were conducted by using a Thermo Scientific Nicolet 5PCFT-IR-ATR spectrophotometer. Zeta potential (Malvern Zetasizer Nano ZSP) measurements were performed in PBS buffer, pH 7.4. Fluorescence measurements were conducted using a Horiba Jobin-Yvon Fluoromax-3 spectrophotometer. These were performed using quartz cuvettes of reduced volume (100 μL). Working wavelengths were set to λ_{exc} = 550 nm and λ_{em} = 555−700 nm to monitor the fluorescence emission of TAMRA, and all measurements were performed at room temperature. Two-photon microscopy images of magnetic beads functionalized with the TAMRA-labeled peptide-PNA translator were acquired by using a vertical Nikon A1R MP+ two-photon microscope equipped with a femtosecond pulsed laser from Coherent Chameleon Discovery.

Loading Curve. DBCO-functionalized magnetic beads (0.1 mg/mL) were incubated with solutions of the fluorescent peptide-PNA of different concentrations (0.01, 0.1, 1, 5, 10, and 24 μM), following the protocol described above. Fluorescence spectroscopy measurements of the peptide-PNA solution before and after incubation with the DBCO-modified magnetic beads were used to calculate the quantity of translators covalently immobilized on the bead surface. The emission intensity of the TAMRA fluorophore conjugated to the peptide-PNA translator was collected in solution at λ_{Em} = 584 nm (λ_{Ex} = 550 nm) before and after the translator immobilization on the magnetic beads. The fluorescence intensity reduction expressed in percentages was used to estimate the number of moles attached to the magnetic beads. The measurements were replicated three times, and the value obtained is reported as the mean value ± standard deviation (Figure S4).

Kinetic Analysis of MMP2-Mediated Proteolytic Cleavage. Magnetic beads functionalized with the fluorescent peptide-PNA translator were incubated with MMP2 (100 nM) for 1, 2, 4, and 8 h, respectively. The supernatant was then collected and analyzed by fluorescence spectroscopy, as described above.[33]

Specificity Assay. MMP1, MMP9, and MMP12 (100 nM solution in TRIS buffer 0.1 M containing $CaCl_2$ 1 mM) were respectively incubated with magnetic beads functionalized with the fluorescent peptide-PNA translator (1 mg/mL) for 2 h at 37 °C. The supernatant was then collected and analyzed by means of fluorescence spectroscopy as described above.

Quantitative Fluorescence-Based Assay. Magnetic beads functionalized with the fluorescent peptide-PNA translator (1 mg/mL) were incubated with varying concentrations of MMP2 in the range 0.03−10 nM (2 h at 37 °C). The supernatant was then collected and analyzed by means of fluorescence spectroscopy as described above. The limit of detection (LOD) was determined according to Eurachem guidelines (https://www.eurachem.org).

CRISPR-Cas12a-Assisted Activity-Based Assays. Magnetic beads covalently conjugated with peptide-PNA translators were prepared as described above (1 mg/mL) and subsequently incubated with a 10 μM solution of the ssDNA activator sequence (2 h at 37 °C) and then washed twice with distilled water. The obtained PNA:DNA-modified beads were incubated with varying concentrations of MMP2 in the range 0.3−300 pM (2 h at 37°). The resulting supernatant was collected and used for subsequent analysis. The LbCas12a-mediated cleavage assays were carried out by adding 7.5 μL of Cas12a/cRNA complex (200 nM, in a buffer consisting of 10 mM Tris-HCl (pH 7.9), 50 mM NaCl, and 100 mM $MgCl_2$) previously incubated (30 min at 37 °C) to 67.5 μL of supernatant solution containing the Hairpin DNA reporter (final concentration 100 nM).[33] Kinetics were followed for 2 h at 37 °C by utilizing a microplate reader Tecan Infinite 200 Pro using top reading mode with black, flat-bottom non-binding 96-well plates. The fluorescence intensity values were expressed in terms of signal gain % (calculated with the following formula: signal gain % = (fluorescence signal − background)/background × 100, where background is the signal observed when conducting the assay in the absence of MMP2) as a function of different MMP2 concentrations and

https://doi.org/10.1021/acs.analchem.4c02622
Anal. Chem. 2024, 96, 18645−18654

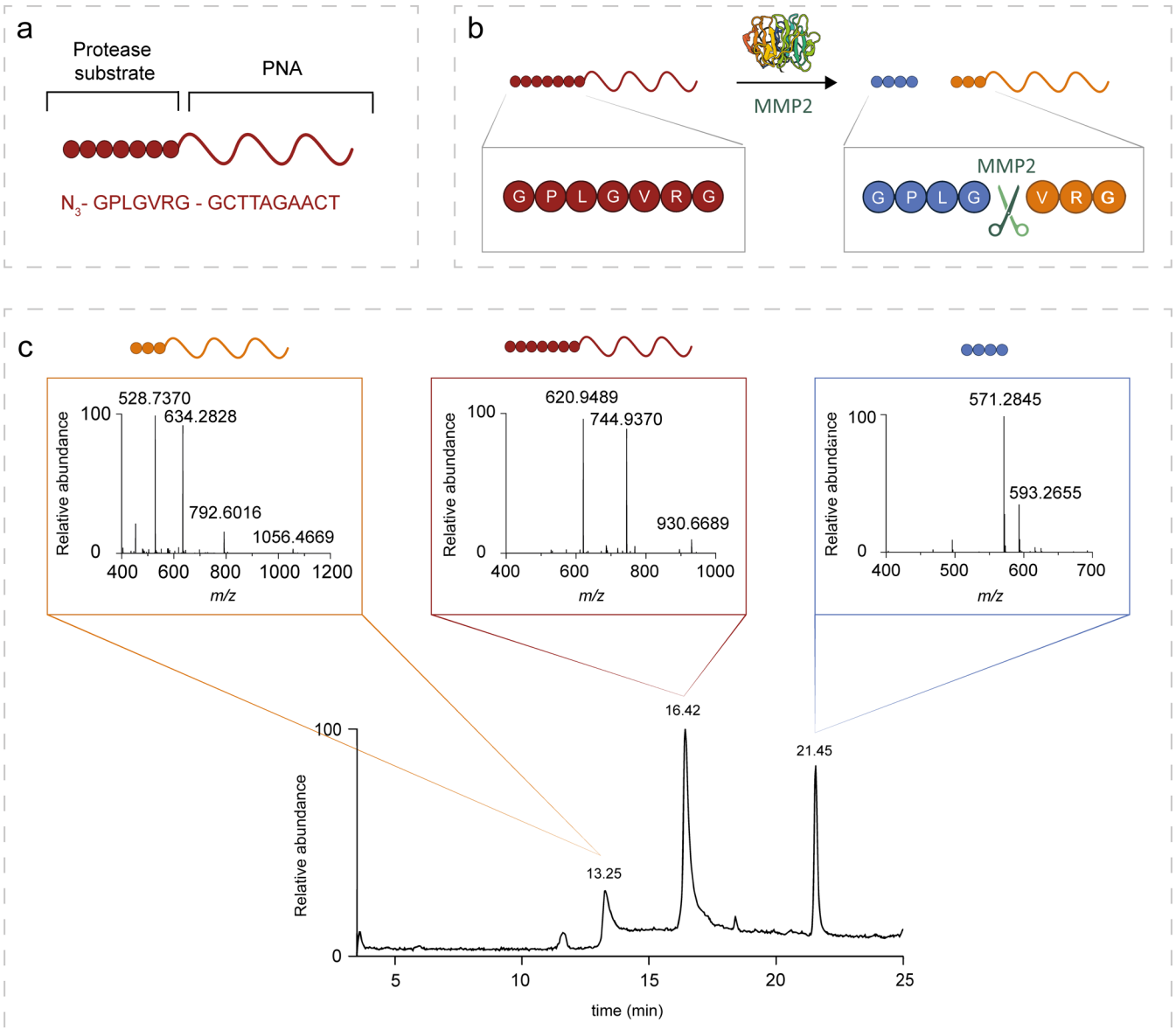

Figure 2. Design of the peptide-PNA chemical translator and HPLC-HRMS analysis of protease cleavage products. (a) Illustration of the molecular design of the chemical translator, reporting the amino acid sequence of the peptide unit and the nucleobase sequence of the PNA unit. An azide group is conjugated to the 5′-end of the probe to enable click chemistry for anchoring to solid supports. A fluorescent version of the translator was obtained by conjugating 5(6)-carboxy-tetramethylrhodamine (TAMRA) to additional lysine residue present at the 3′-end. (b) Schematic representation of the MMP2-mediated enzymatic cleavage of the chemical translator (red circle-line probe), highlighting the cleavage site and the formation of two reaction products, a small peptide fragment (blue circles) and a larger fragment containing the PNA unit (orange circles + orange line). (c) HPLC-ESI-HRMS chromatogram of the chemical translator after incubation with MMP2 (24 h, 37 °C, [MMP2]:[translator] 1:10). The three main peaks correspond to the PNA-containing fragment (rt 13.25 min, m/z = 528.7370 $[M+6H]^{6+}$, 634.2828 $[M+5H]^{5+}$, 792.6016 $[M+4H]^{4+}$, 1056.4669 $[M+3H]^{3+}$ orange box), to unreacted molecular translator present in large excess in the reaction mixture (rt 16.42 min, m/z = 620.9489 $[M+6H]^{6+}$, 744.9370 $[M+5H]^{5+}$, 930.6689 $[M+4H]^{4+}$ red box), and to the peptide fragment (rt 21.45 min, m/z = 571.2845 $[M + H]^{+}$, 593.2655 $[M + Na]^{+}$ blue box).

analyzed using a linear regression model in PRISM (GraphPad).

CRISPR-Cas12a-Assisted Activity-Based Assays in Cell Medium Culture. Magnetic beads covalently conjugated with peptide-PNA translators were prepared as described above (1 mg/mL) and subsequently incubated with a 10 μM solution of the ssDNA activator sequence (2h at 37 °C) and then washed twice with distilled water. The obtained PNA:DNA-modified beads were incubated with varying concentrations of MMP2 in the range of 30−300 pM using DMEMF-12 (1×) as a solvent for this assay. The resulting supernatant was collected and used for subsequent analysis. The LbCas12a-mediated cleavage assays were carried out by adding 7.5 μL of Cas12a/cRNA complex (200 nM, in DMEMF-12 (1×)) previously incubated (30 min at 37 °C) to 67.5 μL of supernatant solution containing the Hairpin DNA reporter (final concentration 100 nM). Kinetics were followed for 2 h at 37 °C by utilizing a Horiba Jobin-Yvon Fluoromax-3 spectrophotometer.

ELISA Protocol for MMP2 Detection. Enzyme-linked sandwich immunoassay (ELISA) as a reference technique for

https://doi.org/10.1021/acs.analchem.4c02622
Anal. Chem. 2024, 96, 18645−18654

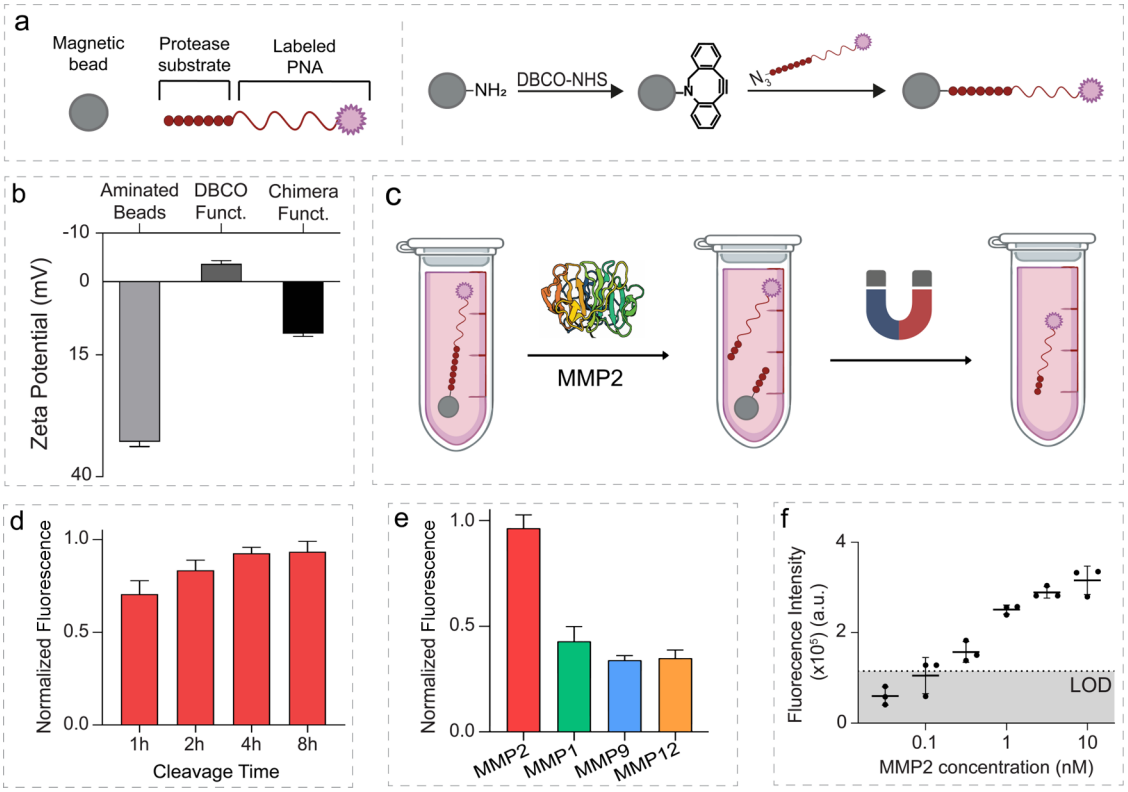

Figure 3. Design of the sensing platform and characterization of the activity-based sensing mechanism. (a) Multistep functionalization scheme of the magnetic beads with the chemical translator. Bifunctional DBCO-NHS allows for conversion of the amine groups initially present on the bead surface into DBCO functionalities. The peptide-PNA translator was then grafted onto these beads through an SPAAC reaction between the azide moiety on the 5′-end of the peptide unit of the translator and DBCO. (b) Zeta potential measurements during the various functionalization steps. After functionalization with DBCO, the zeta potential of a dispersion of the magnetic beads in PBS buffer shifts from 33 ± 1 mV to −4 ± 1 mV. Conjugation with the chemical translator increases the zeta potential to 11 ± 1 mV (n = 3, mean + SD). (c) Illustration of the MMP2 cleavage assay using magnetic beads functionalized with a fluorophore-tagged chemical translator. When the sensing platform is incubated with MMP2, proteolytic cleavage followed by magnetic separation of the beads results in a supernatant enriched in the PNA-containing cleavage product. (d) Normalized fluorescence intensity obtained for the cleavage assay conducted using different MMP2 incubation times ([MMP2] 100 nM, magnetic beads 1 mg/mL, n = 3, mean + SD). (e) Normalized fluorescence intensity obtained with MMP2 (100 nM) and other nonspecific MMPs (100 nM) (n = 3, mean + SD). (f) Fluorescence intensity values obtained for the assay conducted using different concentrations of MMP2 in the range of 0.03−10 nM (cleavage time 2h), from which it was possible to calculate an LOD of 104 pM (n = 3, mean ± SD), calculated as the concentration of MMP2 leading to a signal change equal to 3 times the standard deviation of the background (absence of the target).

the detection of MMP2 was performed following a standard ELISA protocol and colorimetric detection. Commercial multiwell plates were already modified with capture antibody and blocked with BSA to prevent nonspecific interactions. Briefly, 100 μL of sample containing the target (human MMP2) in its corresponding buffer, either incubation buffer or DMEM cell culture buffer, was added to its corresponding well and incubated for 1 h and 30 min at 37 °C. Then, 3 washing cycles were performed, unless otherwise stated, each washing step consisted of cycles of emptying the content in the wells and adding 200 μL per well of washing buffer. Then, 100 μL of biotinylated anti-MMP2 antibody was added to each well and the plates were incubated for 1 h at 37 °C. Next, three washing cycles were performed and 100 μL of Streptavidin-HRP solution was added to each well and incubated for 45 min at 37 °C. Finally, 5 standard washing cycles were performed, then 100 μL of commercial mix of HRP substrate for colorimetric detection was added to each well. The reaction was stopped after 20 min at 37 °C in the dark by the addition of 100 μL of stopping solution. The absorbance signal was read at 450 nm using a Tecan Infinite M200 PRO (Männedorf, Switzerland).

RESULTS AND DISCUSSION

We designed our chemical translator as a peptide-PNA conjugate, where the peptide unit presents the specific substrate sequence of MMP2. We selected the sequence Gly-Pro-Leu-Gly-Val-Arg-Gly, which is reported to be specifically recognized by MMP2 and undergo hydrolytic cleavage of the peptide bond between the Gly-Val residues.[43] The PNA unit directly fused with the above peptide is a linear arbitrary 10-nt-long sequence (Figure 2a). Our choice of using a PNA sequence as the nucleic acid component of the translator was motivated by specific economic and technological advantages over DNA-barcoded peptides. First, it is possible to synthesize the entire translator in a single round of solid-phase synthesis harnessing conventional peptide chemistry, allowing for greatly reduced costs when compared to the synthesis and purchase of peptide−DNA hybrids. Second, DNA-barcoded probes allow for no modularity, meaning that any required change in the DNA sequence involves the fabrication of a whole new hybrid probe. Conversely, using a minimal PNA sequence offers great modularity and versatility because the PNA unit can serve as an anchor for any desired DNA sequence that can simply be hybridized via base pairing, without affecting the design of the

https://doi.org/10.1021/acs.analchem.4c02622
Anal. Chem. 2024, 96, 18645−18654

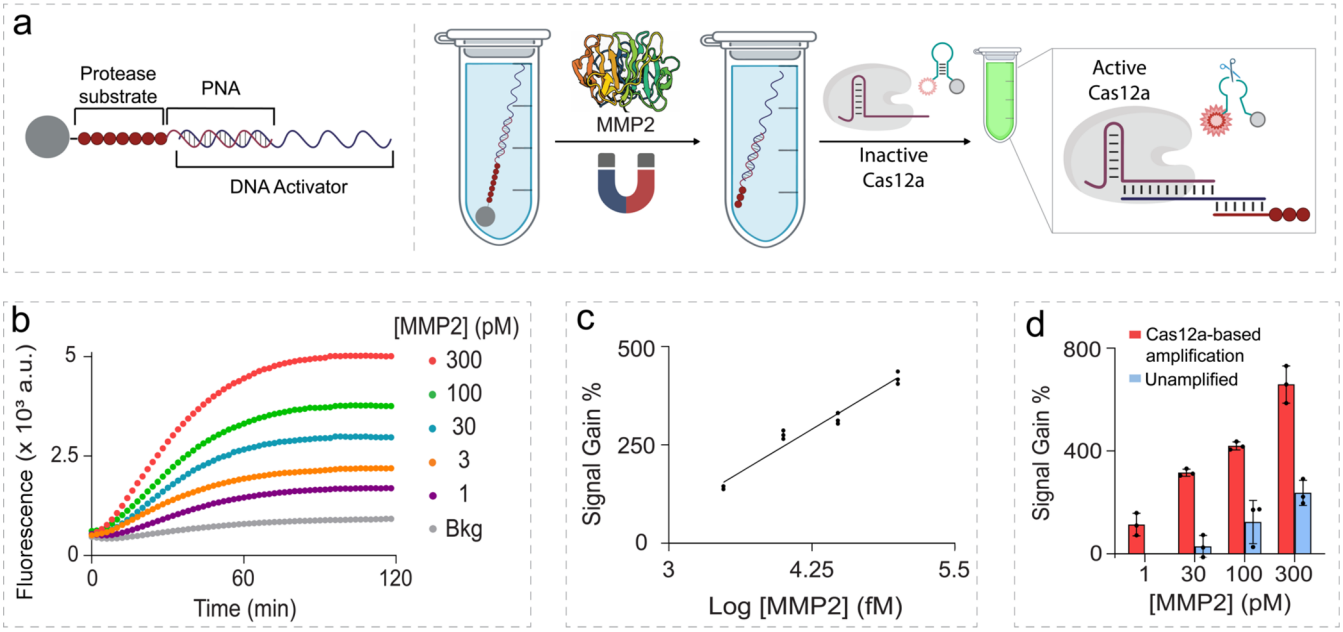

Figure 4. CRISPR-Cas12a-based amplification of MMP2-derived nucleic acid output. (a) Pictorial illustration of the proposed MMP2 activity-based assay using CRISPR-Cas12a-based signal amplification. The peptide-PNA translator on the magnetic bead surface is hybridized with an ssDNA sequence serving as the trigger input for target-induced CRISPR-Cas12 trans-cleavage nuclease activity. Following incubation with MMP2 (2 h) and magnetic separation of the beads, the nucleic acid-containing cleavage product enriches the supernatant. This is incubated with a preformed crRNA/Cas12a complex (20 nM) in the presence of an excess of ssDNA hairpin reporter (100 nM). (b) Fluorescence kinetic profiles of CRISPR-Cas12a trans-cleavage activity (i.e., Cas12a-mediated degradation of the DNA hairpin reporters) upon interaction with MMP2-derived ssDNA activator in the MMP2 concentration range 1−300 pM. (c) Calibration curve obtained through a linear fit of signal gain % values in the 3−100 pM MMP2 concentration range. The curve is described by the following equation: $y = (-452.1 \pm 48.7) + (174.6 \pm 11.4)x$, $R^2 = 0.96$. (d) Signal gain % values, calculated at the 2 h end point, obtained for CRISPR-Cas12a-based (red bars) and unamplified fluorescence assays (blue bars) for different concentrations of MMP2 ($n = 3$, mean ± SD).

PNA-peptide translator. Given the exceptional stability of PNA:DNA duplexes,[44,45] this relatively short PNA sequence can be used as an anchor for hybridization with the CRISPR-Cas12a target ssDNA, showing a melting temperature of around 64 °C (Figure S1). This facilitates synthesis and minimizes the length of the duplex region in the fragment of the translator, serving as the new input for CRISPR-Cas12a (Figure 1), therefore limiting possible steric hindrance effects. In addition, we included an azide group on the 5′-end of the translator to enable click chemistry for the immobilization of the probe on a solid support (Figure 2a). The peptide-PNA translator was synthesized using conventional FMOC-based solid-phase chemistry and purified via HPLC, and its identity was confirmed using mass spectrometry (see Supporting Information, Figures S2 and S3). To validate the functionality of our synthetic probe as a substrate for MMP2, we demonstrated hydrolysis of the peptide unit at the anticipated cleavage site. After incubating the translator and the protease together, we analyzed the reaction products by means of HPLC-ESI-HRMS (Figure 2b,c). As shown in Figure 2c, one peak in the chromatogram corresponded to the unreacted translator, which was used in large excess in this experiment, and the other two main peaks could be associated with the two expected fragments generated from hydrolytic cleavage of the peptide unit, thus confirming that the peptide-PNA translator can effectively serve as a synthetic substrate for MMP2 (Figure 2c).

We resorted to magnetic beads as solid platforms for the physical anchoring of the chemical translator. This enables isolation of the cleaved PNA-containing fragment, serving as a nucleic acid-based input for further signal elaboration. We employed micrometer-sized magnetic beads functionalized with amine groups on their surfaces. We chose to covalently immobilize the translator onto the beads through a copper-free strain-promoted alkyne−azide cycloaddition (SPAAC) reaction, which has the advantage of being orthogonal to all of the other reactive groups in the peptide-PNA sequence. To do so, we first transformed the amine groups on the bead surface into SPAAC-reactive cyclooctyne groups by reacting them with dibenzocyclooctyne-*N*-hydroxysuccinimidyl ester (DBCO-NHS) (Figure 3a). Zeta potential measurements of the changes in the net surface charge of the magnetic beads after treatment with different concentrations of DBCO-NHS were used to study and optimize the functionalization reaction (Figure S4). We then explored the most advantageous conditions for the SPAAC reaction by evaluating different solvents (see Supporting Information, Table S1).[46] To validate the presence of the translator on the magnetic bead surface, we used a version of the translator labeled with tetramethylrhodamine (TAMRA). This allowed us to calculate the quantity of translator immobilized on the beads by means of fluorescence spectroscopy (Figure S5 and Table S1). Conducting the SPAAC reaction in TRIS buffer enabled the construction of a loading curve for standardizing the surface probe density, showing that a solution of 10 μM peptide-PNA conjugate was required to maximize the efficiency of the functionalization process, affording 7.68 nmol of translator attached per mg of magnetic beads (Figure S6). Characterization of the different functionalization steps was performed by means of zeta potential measurements, ATR-FT-IR spectroscopy, and two-

https://doi.org/10.1021/acs.analchem.4c02622
Anal. Chem. 2024, 96, 18645−18654

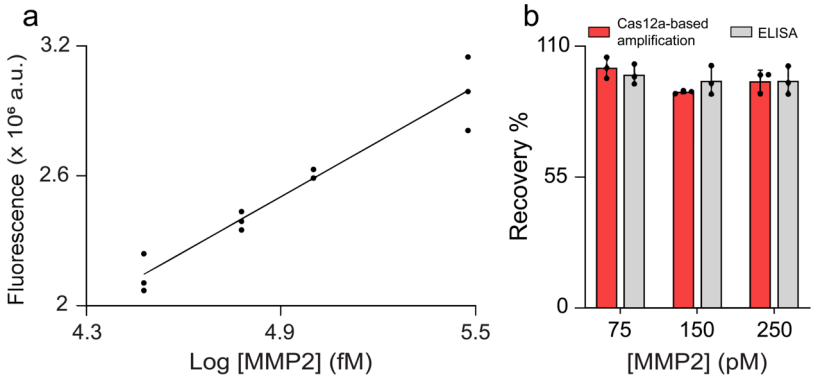

Figure 5. Analysis of MMP2 in undiluted cell culture medium. (a) Calibration curve obtained through a linear fit of fluorescence intensity values in the 30−300 pM MMP2 concentration range using spiked samples in undiluted DMEM cell culture medium. The curve is described by the following equation: $y = (-1{,}660{,}085 \pm 353{,}763) + (849{,}889 \pm 71{,}517)x$, $R^2 = 0.93$. (b) Recovery values for different concentrations of MMP2 in undiluted DMEM cell culture medium when using the developed CRISPR-Cas assay or a commercially available standard ELISA ($n = 3$, mean ± SD).

photon fluorescence microscopy (Figures 3b, S7, and S8). Next, we demonstrated that MMP2 could effectively hydrolyze the peptide-PNA translator anchored on the magnetic bead surface. To this end, we functionalized the magnetic beads with a fluorescent TAMRA-labeled version of the translator (see the SI). After incubation with MMP2 and magnetic separation of the beads, it was possible to detect and quantify the TAMRA-labeled PNA-containing cleavage product in the supernatant by using fluorescence spectroscopy (Figure 3c). Based on the fluorescence emission intensity of the supernatant, the cleavage process effectively occurred in 2 h, which aligns with what is reported for other activity-based sensing platforms for MMP2 (Figure 3d).[47] We also evaluated the specificity of our sensing platform for MMP2 when exposed to other proteases from the MMP family, namely, MMP1, MMP9, and MMP12. As reported in the literature, some level of cross-reactivity could be observed in this case, which was also observed in our experimental results (Figure 3d).[48] Potential substrate cross-over for different members of the MMP family is not unexpected, as these proteases tend to show a poor substrate sequence specificity, making it difficult to use a peptide substrate alone to differentiate the activity of a particular MMP from others.[49−52] We selected the current sequence GPLGVRG for our chemical translator because this is one of the well-characterized substrates preferentially cleaved by MMP2, despite its being also potentially susceptible to other proteases.[53,54] The main goal of our work was to demonstrate a general proof-of-principle strategy for applying CRISPR-Cas12a signal amplification to a target protease through an input exchange mechanism, and this motivated us to utilize a peptide sequence known to ensure efficient MMP cleavage. Fluorescence spectroscopy measurements of the supernatant after physical separation of the translator-modified beads showed that the sensing platform exhibited substantial specificity for MMP2 (Figure 3e). Quantitative analysis of the concentration of the TAMRA-labeled PNA-containing cleavage product in the supernatant after incubation of the functionalized magnetic beads (1 mg/mL, equivalent to 10 μM translator in 150 μL of assay volume) with varying concentrations of MMP2 allowed us to estimate a limit of detection (LOD) of 104 pM for the current nonamplified sensing platform (Figure 3f).

Next, to achieve translation of MMP2 enzymatic activity into a DNA-based input for the activation of CRISPR-Cas12a, we integrated a strategy for protein-to-DNA input exchange into the sensing platform. Signal amplification based on the use of CRISPR-Cas12a leverages the target-induced indiscriminate nuclease activity (trans-cleavage) of Cas12a, which can be used for degrading nearby single-stranded DNA reporter labeled with a fluorophore/quencher pair.[33,55,56] CRISPR-Cas12a can recognize either complementary single-stranded (ss) or double-stranded (ds) DNA sequences.[57] We designed an ssDNA sequence encompassing both a domain complementary to the sequence of the PNA unit in the translator and a second domain serving as the target sequence for the crRNA complexed with Cas12a (Figure 4a and SI). By preforming the PNA:DNA heteroduplex on the magnetic bead surface, the sensing platform could release the DNA-containing fragment in the supernatant, following MMP2-mediated cleavage of the translator (Figure 4a). The hybridization between the crRNA in the CRISPR-Cas12a complex and its target ssDNA in the supernatant activates the trans-endonuclease activity of Cas12a, allowing to generate an amplified fluorescence signal through the indiscriminate degradation of hairpin DNA reporters labeled with a FAM/BHQ fluorophore/quencher pair. We chose to employ hairpin DNA reporters based on a recent publication demonstrating that such conformation enables greatly enhanced sensitivity compared to the conventional linear DNA reporters routinely utilized in other CRISPR-Cas assays.[33] Figure 4b reports representative kinetic fluorescence measurements of MMP2-dependent Cas12a-mediated degradation of the hairpin reporters, showing that the amplification process proceeds to completion in less than 2 h. We note that a gradual, albeit slight, increase in the signal of the blank group can be observed. This phenomenon can be primarily attributed to a residual fraction of modified magnetic beads remaining in the supernatant after magnetic separation. This results in a small excess of activator DNA in the supernatant, which can likely be recognized by the CRISPR-Cas12a complex and triggers the generation of the observed background signal. One potential solution for reducing leakage of the DNA activator would be integrating it in a peptide−DNA conjugate, although this would make synthesis more difficult and expensive and eliminate the possibility of a modular system. The end point fluorescence intensity values were used to build a calibration curve that showed linearity in the MMP2 concentration range of 3−100 pM, with an LOD of 1 pM, corresponding to 72 pg/mL MMP2 (Figure 4c). This

https://doi.org/10.1021/acs.analchem.4c02622
Anal. Chem. 2024, 96, 18645−18654

LOD is orders of magnitude lower than average commercially available peptide-based kits, and it is also lower than the LOD value of 59 pM reported for a recently published activity-based CRISPR-Cas assay leveraging DNA-barcoded platforms.[58] Our presented assay also performs very well when compared to systems based on CRET[59] and BRET,[60] which have reported LOD, respectively, of 0.5 nM and 12.5 pM. Figure 4d reports signal gain % values calculated for different concentrations of MMP2 after CRISPR-Cas12a-based processing of the MMP2-derived nucleic acid output. The resulting signal amplification leads to a significant increase in the signal gain % values with respect to those that can be calculated from the nonamplified fluorescence intensity values reported in Figure 3c.

Next, we assessed the performance of our CRISPR-Cas12a protease assay in the relevant biological matrix for MMP2 for *in vitro* assays, i.e., cell culture medium, which is where MMP2 is mainly found after being secreted by cells in the surrounding environment.[18,21,61,62] By using spiked samples of MMP2 in undiluted DMEM cell culture medium, we could build a calibration curve that showed linearity in the MMP2 concentration range 30−300 pM, with a LOD of 23 pM, corresponding to 1.7 ng/mL MMP2 (Figure 5a). This observed change in the range of the calibration curve and the corresponding shift in the LOD when compared to model buffer conditions are indicative of a matrix interference effect caused by the complexity of the DMEM cell culture. A similar increase in the LOD was reported for other protease activity-based assays when deployed to complex biological matrices.[37] An analogous effect was also observed when applying a reference method based on a commercially available ELISA to the same spiked samples of MMP2 in undiluted DMEM cell culture (Figure S9). To assess the accuracy of our CRISPR-based assay with respect to that of this standard ELISA kit, we conducted a spike and recovery assessment through quantification of MMP2 in undiluted DMEM using both assays. Specifically, spiked DMEM samples were prepared at three different standard concentrations (75, 150, and 250 pM). Our CRISPR-based assay successfully identified these concentrations with average recoveries ranging from 95 to 101%, in agreement with the values obtained with the standard ELISA (Figure 5b and Table S9 in the SI). Good precision was also observed with a relative standard deviation (RSD%) of less than 6% for each tested MMP2 concentration. Taken all together, these results are quite remarkable when compared with the analytical performance of commercially available fluorogenic kits, such as SensoLyte from AnaSpec, declaring an LOD of 15 ng/mL, and InnoZyme from Merck-Millipore, declaring an LOD of 20 ng/mL.[63,64]

CONCLUSIONS

In conclusion, we successfully developed a novel sensing platform for the activity-based detection of MMP2, enabled by a protein-to-DNA input exchange mechanism combined with a CRISPR-Cas12a signal amplification. The presented strategy showcases a new application space for CRISPR-Cas-based biosensing, highlighting its potential beyond nucleic acid diagnostics.[65,66] Our CRISPR-Cas12a-assisted sensing platform demonstrated remarkable sensitivity and an LOD as low as 72 pg/mL MMP2, outperforming commercially available activity-based fluorogenic kits. The ability of this sensing platform to work in undiluted cell culture medium with an LOD of 23 pM suggests its potential for *in vitro* diagnostics and drug screening assays. Further studies with clinical samples will be needed to explore its potential as a diagnostic platform. Key in our design is the use of a chimeric peptide-PNA conjugate, serving as a molecular translator for the conversion of an enzyme-based input into a nucleic acid-based output. The nature of the translator allows for adaptation to the detection of other specific MMPs and enzymes simply by modifying the peptide substrate sequence, making the presented strategy a highly versatile platform technology for the realization of CRISPR-Cas-based detection of protein targets. High specificity for particular proteases can be obtained by employing optimal peptide substrate sequences.[67,68] As this approach enables the generation of a protein-derived arbitrary nucleic acid-based input, many other amplification techniques, such as those based on CRISPR-Cas13, hybridization chain reaction, or polymerase chain reaction, could be explored, also opening the possibility to perform multiplexing biomarker analysis. From a different angle, this work also demonstrates a new possible modality for enzyme-controlled DNA-based computation, enabling the integration of proteolytic activity with DNA nanotechnology.[26,69−72]

ASSOCIATED CONTENT

Supporting Information

The Supporting Information is available free of charge at https://pubs.acs.org/doi/10.1021/acs.analchem.4c02622.

Materials, nucleic acid sequences, including those of the PNA-peptide translator, a description of the experimental conditions for SPAAC reaction; FT-IR spectra, fluorescence emission spectra, zeta potential measurements, chromatogram for the peptide-PNA conjugate characterization, two-photon microscopy image of functionalized magnetic beads, and experimental results from ELISA (PDF)

AUTHOR INFORMATION

Corresponding Author

Alessandro Bertucci − *Department of Chemistry, Life Sciences and Environmental Sustainability, University of Parma, 43124 Parma, Italy*; orcid.org/0000-0003-4842-9909; Email: alessandro.bertucci@unipr.it

Authors

Luca Capelli − *Department of Chemistry, Life Sciences and Environmental Sustainability, University of Parma, 43124 Parma, Italy*

Federica Pedrini − *Department of Chemistry, Life Sciences and Environmental Sustainability, University of Parma, 43124 Parma, Italy*

Andrea C. Di Pede − *Department of Chemistry, University of Rome Tor Vergata, 00133 Rome, Italy*

Alejandro Chamorro-Garcia − *Department of Chemistry, University of Rome Tor Vergata, 00133 Rome, Italy*

Neda Bagheri − *Department of Chemistry, University of Rome Tor Vergata, 00133 Rome, Italy*; orcid.org/0009-0005-0805-8201

Simone Fortunati − *Department of Chemistry, Life Sciences and Environmental Sustainability, University of Parma, 43124 Parma, Italy*

Marco Giannetto − *Department of Chemistry, Life Sciences and Environmental Sustainability, University of Parma, 43124 Parma, Italy*; orcid.org/0000-0001-7031-7466

Monica Mattarozzi − *Department of Chemistry, Life Sciences and Environmental Sustainability, University of Parma, 43124 Parma, Italy;* orcid.org/0000-0002-6766-4616
Roberto Corradini − *Department of Chemistry, Life Sciences and Environmental Sustainability, University of Parma, 43124 Parma, Italy;* orcid.org/0000-0002-8026-0923
Alessandro Porchetta − *Department of Chemistry, University of Rome Tor Vergata, 00133 Rome, Italy;* orcid.org/0000-0002-4061-5574

Complete contact information is available at: https://pubs.acs.org/10.1021/acs.analchem.4c02622

Author Contributions

§L.C. and F.P. contributed equally. The manuscript was written through contributions of all authors. All authors have given approval to the final version of the manuscript.

Notes

The authors declare no competing financial interest.

■ ACKNOWLEDGMENTS

This research was granted by University of Parma through the action Bando di Ateneo 2022 per la ricerca cofunded by MUR-Italian Ministry of Universities and Research−D.M. 737/2021-PNR-PNRR-NextGenerationEU. This work was supported by the Guido Berlucchi Foundation Mini Grant codice progetto BERTUCCI_2022_FONDBERLUCCHI. A.B. and A.P. acknowledge financial support under the National Recovery and Resilience Plan (NRRP), Mission 4, Component 2, Investment 1.1, Call for tender No. 104 published on 2.2.2022 by the Italian Ministry of University and Research (MUR), funded by the European Union − NextGenerationEU− Project Title "CRISPR-Cas-based sensing platforms for the monitoring of clinically relevant antibodies"− CUP D53D23009090001-Project Code 2022FPYZ2N - Grant Assignment Decree No. 958 adopted on 30-06-2023 by the Italian Ministry of Ministry of University and Research (MUR). This work has benefited from the equipment and framework of the COMP-HUB and COMP-R Initiatives, funded by the "Departments of Excellence" program of the Italian Ministry for University and Research (MIUR, 2018-2022 and MUR, 2023-2027).

■ REFERENCES

(1) Soleimany, A. P.; Bhatia, S. N. *Trends Mol. Med.* **2020**, *26* (5), 450−468.
(2) Muir, R. K.; Guerra, M.; Bogyo, M. M. *ACS Chem. Biol.* **2022**, *17* (2), 281−291.
(3) Kandell, R. M.; Kudryashev, J. A.; Kwon, E. J. *ACS Nano* **2021**, *15* (12), 20504−20516.
(4) Kudryashev, J. A.; Madias, M. I.; Kandell, R. M.; Lin, Q. X.; Kwon, E. J. *Adv. Funct. Mater.* **2023**, *33* (28), 2300218 DOI: 10.1002/adfm.202300218.
(5) Nagano, N.; Ichihashi, Y.; Komatsu, T.; Matsuzaki, H.; Hata, K.; Watanabe, T.; Misawa, Y.; Suzuki, M.; Sakamoto, S.; Kagami, Y.; Kashiro, A.; Takeuchi, K.; Kanemitsu, Y.; Ochiai, H.; Watanabe, R.; Honda, K.; Urano, Y. *Chem. Sci.* **2023**, *14* (17), 4495−4499.
(6) Sanman, L. E.; Bogyo, M. *Annu. Rev. Biochem.* **2014**, *83*, 249−273.
(7) Zmudzinski, M.; Malon, O.; Poręba, M.; Drąg, M. *Curr. Opin. Chem. Biol.* **2023**, *74*, 102299.
(8) Zhang, H.; Wu, M.; Ta, H. T.; Xu, Z. P.; Zhang, R. *Adv. Mater. Technol.* **2023**, *8*, 2201786 DOI: 10.1002/admt.202201786.
(9) Ćwilichowska, N.; Świderska, K. W.; Dobrzyń, A.; Drąg, M.; Poręba, M. *Mol. Aspects Med.* **2022**, *88*, 101144.
(10) Dudani, J. S.; Warren, A. D.; Bhatia, S. N. *Annu. Rev. Cancer Biol.* **2018**, *2*, 353−376.
(11) Egeblad, M.; Werb, Z. *Nat. Rev. Cancer* **2002**, *2* (3), 161−174.
(12) Quintero-Fabián, S.; Arreola, R.; Becerril-Villanueva, E.; Torres-Romero, J. C.; Arana-Argáez, V.; Lara-Riegos, J.; Ramírez-Camacho, M. A.; Alvarez-Sánchez, M. E. *Front. Oncol.* **2019**, *9*, 1370 DOI: 10.3389/fonc.2019.01370.
(13) Gobin, E.; Bagwell, K.; Wagner, J.; Mysona, D.; Sandirasegarane, S.; Smith, N.; Bai, S.; Sharma, A.; Schleifer, R.; She, J. X. *BMC Cancer* **2019**, *19* (1), 1−10, DOI: 10.1186/s12885-019-5768-0.
(14) Fields, G. B. Using Fluorogenic Peptide Substrates to Assay Matrix Metalloproteinases. In *Matrix Metalloproteinase Protocols*; Clark, I. M.; Young, D. A.; Rowan, A. D., Eds.; Humana Press, 2010; Vol. *622*, pp 393−433.
(15) Pham, W.; Choi, Y.; Weissleder, R.; Tung, C. H. *Bioconjugate Chem.* **2004**, *15* (6), 1403−1407.
(16) Ryu, J. H.; Lee, A.; Lee, S.; Ahn, C. H.; Park, J. W.; Leary, J. F.; Park, S.; Kim, K.; Kwon, I. C.; Youn, I. C.; Choi, K. *Bioconjugate Chem.* **2010**, *21* (7), 1378−1384.
(17) Li, X.; Deng, D.; Xue, J.; Qu, L.; Achilefu, S.; Gu, Y. *Biosens. Bioelectron.* **2014**, *61*, 512−518.
(18) Feng, D.; Zhang, Y.; Feng, T.; Shi, W.; Li, X.; Ma, H. *Chem. Commun.* **2011**, *47* (38), 10680−10682.
(19) Welser, K.; Adsley, R.; Moore, B. M.; Chan, W. C.; Aylott, J. W. *Analyst* **2011**, *136* (1), 29−41.
(20) Jin, Z.; Dridi, N.; Palui, G.; Palomo, V.; Jokerst, J. V.; Dawson, P. E.; Sang, Q. X. A.; Mattoussi, H. *Anal. Chem.* **2023**, *95* (5), 2713−2722.
(21) Lei, Z.; Zhang, H.; Wang, Y.; Meng, X.; Wang, Z. *Anal. Chem.* **2017**, *89* (12), 6749−6757.
(22) Biela, A.; Watkinson, M.; Meier, U. C.; Baker, D.; Giovannoni, G.; Becer, C. R.; Krause, S. *Biosens. Bioelectron.* **2015**, *68*, 660−667.
(23) Kou, B. B.; Chai, Y. Q.; Yuan, Y. L.; Yuan, R. *Anal. Chem.* **2017**, *89* (17), 9383−9387.
(24) Li, Y.; Liu, W.; Xu, Q.; Hu, J.; Zhang, C.-y. *Biosens. Bioelectron.* **2020**, *169*, 112647 DOI: 10.1016/j.bios.2020.112647.
(25) Luo, X.; Zhao, J.; Xie, X.; Liu, F.; Zeng, P.; Lei, C.; Nie, Z. *Anal. Chem.* **2020**, *92* (24), 16314−16321.
(26) Bui, H.; Brown, C. W.; Buckhout-White, S.; Díaz, S. A.; Stewart, M. H.; Susumu, K.; Oh, E.; Ancona, M. G.; Goldman, E. R.; Medintz, I. L. *Small* **2019**, *15* (14), 1805384 DOI: 10.1002/smll.201805384.
(27) Yang, M.; Shi, K.; Liu, F.; Kang, W.; Lei, C.; Nie, Z. *Sci. China Chem.* **2021**, *64* (2), 330−336.
(28) Liu, F.; Yang, M.; Song, W.; Luo, X.; Tang, R.; Duan, Z.; Kang, W.; Xie, S.; Liu, Q.; Lei, C.; Huang, Y.; Nie, Z.; Yao, S. *Chem. Sci.* **2020**, *11* (11), 2993−2998.
(29) Kaminski, M. M.; Abudayyeh, O. O.; Gootenberg, J. S.; Zhang, F.; Collins, J. J. *Nat. Biomed. Eng.* **2021**, *5* (7), 643−656.
(30) Li, S. Y.; Cheng, Q. X.; Li, X. Y.; Zhang, Z. L.; Gao, S.; Cao, R. B.; Zhao, G. P.; Wang, J.; Wang, J. M. *Cell Discovery* **2018**, *4* (1), 20 DOI: 10.1038/s41421-018-0028-z.
(31) Chen, J. S.; Ma, E.; Harrington, L. B.; Da Costa, M.; Tian, X.; Palefsky, J. M.; Doudna, J. A. *Science* **2018**, *360*, 436−439.
(32) Broughton, J. P.; Deng, X.; Yu, G.; Fasching, C. L.; Servellita, V.; Singh, J.; Miao, X.; Streithorst, J. A.; Granados, A.; Sotomayor-Gonzalez, A.; Zorn, K.; Gopez, A.; Hsu, E.; Gu, W.; Miller, S.; Pan, C. Y.; Guevara, H.; Wadford, D. A.; Chen, J. S.; Chiu, C. Y. *Nat. Biotechnol.* **2020**, *38* (7), 870−874.
(33) Rossetti, M.; Merlo, R.; Bagheri, N.; Moscone, D.; Valenti, A.; Saha, A.; Arantes, P. R.; Ippodrino, R.; Ricci, F.; Treglia, I.; Delibato, E.; Van Der Oost, J.; Palermo, G.; Perugino, G.; Porchetta, A. *Nucleic Acids Res.* **2022**, *50* (14), 8377−8391.
(34) Li, J.; Yang, S.; Zuo, C.; Dai, L.; Guo, Y.; Xie, G. *ACS Sens.* **2020**, *5* (4), 970−977.
(35) Xiong, Y.; Zhang, J.; Yang, Z.; Mou, Q.; Ma, Y.; Xiong, Y.; Lu, Y. *J. Am. Chem. Soc.* **2020**, *142* (1), 207−213.

(36) Hao, L.; Zhao, R. T.; Welch, N. L.; Tan, E. K. W.; Zhong, Q.; Harzallah, N. S.; Ngambenjawong, C.; Ko, H.; Fleming, H. E.; Sabeti, P. C.; Bhatia, S. N. *Nat. Nanotechnol.* **2023**, *18* (7), 798−807.
(37) Kang, W.; Xiao, F.; Zhu, X.; Ling, X.; Xie, S.; Li, R.; Yu, P.; Cao, L.; Lei, C.; Qiu, Y.; Liu, T.; Nie, Z. *Angew. Chem., Int. Ed.* **2024**, *63* (16), e202400599 DOI: 10.1002/anie.202400599.
(38) Pandit, S.; Duchow, M.; Chao, W.; Capasso, A.; Samanta, D. *Angew. Chem., Int. Ed.* **2024**, *63*, e202310964 DOI: 10.1002/anie.202310964.
(39) Dutta, A.; Li, J.; Lu, H.; Akech, J.; Pratap, J.; Wang, T.; Zerlanko, B. J.; Gerald, T. J. F.; Jiang, Z.; Birbe, R.; Wixted, J.; Violette, S. M.; Stein, J. L.; Stein, G. S.; Lian, J. B.; Languino, L. R. *Cancer Res.* **2014**, *74* (5), 1598−1608.
(40) Tuszynski, G.; Jhon, A. *Pathol. Oncol. Res.* **2001**, *7*, 14−23.
(41) Xie, T. X.; Wei, D.; Liu, M.; Gao, A. C.; Ali-Osman, F.; Sawaya, R.; Huang, S. *Oncogene* **2004**, *23* (20), 3550−3560.
(42) Jezierska, A.; Motyl, T. *Med. Sci. Monit.* **2009**, *15* (2), RA32−RA40.
(43) Von Maltzahn, G.; Harris, T. J.; Park, J. H.; Min, D. H.; Schmidt, A. J.; Sailor, M. J.; Bhatia, S. N. *J. Am. Chem. Soc.* **2007**, *129* (19), 6064−6065.
(44) Jensen, K. K.; Ørum, H.; Nielsen, P. E.; Nordén, B. *Biochemistry* **1997**, *36* (16), 5072−5077.
(45) Egholm, M.; Buchardt, O.; Christensen, L.; Behrens, C.; Freier, S. M.; Driver, D. A.; Berg, R. H.; Kim, S. K.; Norden, B.; Nielsen, P. E. *Nature* **1993**, *365* (6446), 566−568.
(46) Davis, D. L.; Price, E. K.; Aderibigbe, S. O.; Larkin, M. X. H.; Barlow, E. D.; Chen, R.; Ford, L. C.; Gray, Z. T.; Gren, S. H.; Jin, Y.; Keddington, K. S.; Kent, A. D.; Kim, D.; Lewis, A.; Marrouche, R. S.; O'Dair, M. K.; Powell, D. R.; Scadden, M. H. C.; Session, C. B.; Tao, J.; Trieu, J.; Whiteford, K. N.; Yuan, Z.; Yun, G.; Zhu, J.; Heemstra, J. M. *J. Org. Chem.* **2016**, *81* (15), 6816−6819.
(47) Liu, L.; Chu, H.; Yang, J.; Sun, Y.; Ma, P.; Song, D. *Biosens. Bioelectron.* **2022**, *212*, 114389.
(48) Yin, L.; Sun, H.; Zhang, H.; He, L.; Qiu, L.; Lin, J.; Xia, H.; Zhang, Y.; Ji, S.; Shi, H.; Gao, M. *J. Am. Chem. Soc.* **2019**, *141* (7), 3265−3273.
(49) Nagase, H.; Ogata, Y.; Suzuki, K.; Enghild, J. J.; Salvesen, G. *Biochem. Soc. Trans.* **1991**, *19*, 715−718.
(50) Kwong, G. A.; Von Maltzahn, G.; Murugappan, G.; Abudayyeh, O.; Mo, S.; Papayannopoulos, I. A.; Sverdlov, D. Y.; Liu, S. B.; Warren, A. D.; Popov, Y.; Schuppan, D.; Bhatia, S. N. *Nat. Biotechnol.* **2013**, *31* (1), 63−70.
(51) Schuerle, S.; Dudani, J. S.; Christiansen, M. G.; Anikeeva, P.; Bhatia, S. N. *Nano Lett.* **2016**, *16* (10), 6303−6310.
(52) Xie, J.; Zhang, F.; Aronova, M.; Zhu, L.; Lin, X.; Quan, Q.; Liu, G.; Zhang, G.; Choi, K. Y.; Kim, K.; Sun, X.; Lee, S.; Sun, S.; Leapman, R.; Chen, X. *ACS Nano* **2011**, *5* (4), 3043−3051.
(53) Ke, W.; Zha, Z.; Mukerabigwi, J. F.; Chen, W.; Wang, Y.; He, C.; Ge, Z. *Bioconjugate Chem.* **2017**, *28* (8), 2190−2198.
(54) Harris, T. J.; Von Maltzahn, G.; Derfus, A. M.; Ruoslahti, E.; Bhatia, S. N. *Angew. Chem., Int. Ed.* **2006**, *45* (19), 3161−3165.
(55) Li, S.-Y.; Cheng, Q.-X.; Liu, J.-K.; Nie, X.-Q.; Zhao, G.-P.; Wang, J. *Cell Res.* **2018**, *28*, 491−493, DOI: 10.1038/s41422-018.
(56) Wang, B.; Wang, R.; Wang, D.; Wu, J.; Li, J.; Wang, J.; Liu, H.; Wang, Y. *Anal. Chem.* **2019**, *91* (19), 12156−12161.
(57) Feng, W.; Newbigging, A. M.; Tao, J.; Cao, Y.; Peng, H.; Le, C.; Wu, J.; Pang, B.; Li, J.; Tyrrell, D. L.; Zhang, H.; Le, X. C. *Chem. Sci.* **2021**, *12* (13), 4683−4698.
(58) (a) https://www.anaspec.com/en/catalog/sensolyte-520-mmp-2-assay-kit-fluorimetric-1-kit~9d6616da-4170-4e04-93d7-9bdcd084a456. (b) https://bpsbioscience.com/fluorogenic-mmp2-assay-kit-79918.
(59) Hananya, N.; Press, O.; Das, A.; Scomparin, A.; Satchi-Fainaro, R.; Sagi, I.; Shabat, D. *Chem.—Eur. J.* **2019**, *25* (64), 14679−14687.
(60) den Hamer, A.; Den Dierickx, P.; Arts, R.; De Vries, J. S. P. M.; Brunsveld, L.; Merkx, M. *ACS Sens.* **2017**, *2* (6), 729−734.
(61) Jian, M.; Su, M.; Gao, J.; Wang, Z. Peptide Microarray-Based Fluorescence Assay for Quantitatively Monitoring the Tumor-Associated Matrix Metalloproteinase-2 Activity. *Sens. Actuators B Chem.* **2020**, *304*. 127320.
(62) Chan, Y. C.; Chen, C. W.; Chan, M. H.; Chang, Y. C.; Chang, W. M.; Chi, L. H.; Yu, H. M.; Lin, Y. F.; Tsai, D. P.; Liu, R. S.; Hsiao, M. *Biosens. Bioelectron.* **2016**, *80*, 131−139.
(63) https://www.merckmillipore.com/IT/it/product/InnoZyme-Gelatinase-MMP-2-MMP-9-Activity-Assay-kit-Fluorogenic,EMD_BIO-CBA003?ReferrerURL=https%3A%2F%2Fwww.google.com%2F.
(64) https://www.anaspec.com/en/catalog/sensolyte-520-mmp-2-assay-kit-fluorimetric-1-kit~9d6616da-4170-4e04-93d7-9bdcd084a456.
(65) Bruch, R.; Urban, G. A.; Dincer, C. *Trends Biotechnol.* **2019**, *37* (8), 791−792.
(66) Phan, Q. A.; Truong, L. B.; Medina-Cruz, D.; Dincer, C.; Mostafavi, E. *Biosens. Bioelectron.* **2022**, *197*, 113732.
(67) Boulware, K. T.; Daugherty, P. S. *Proc. Natl. Acad. Sci. U.S.A.* **2006**, *103* (20), 7583−7588.
(68) Harris, J. L.; Backes, B. J.; Leonetti, F.; Mahrus, S.; Ellman, J. A.; Craik, C. S. *Proc. Natl. Acad. Sci. U.S.A.* **2000**, *97* (14), 7754−7759.
(69) Bertucci, A.; Porchetta, A.; Grosso, E.; Del Patiço, A.; Idili, A.; Ricci, F. *Angew. Chem., Int. Ed.* **2020**, *59*, 20577−20581.
(70) Bucci, J.; Irmisch, P.; Del Grosso, E.; Seidel, R.; Ricci, F. *J. Am. Chem. Soc.* **2022**, *144* (43), 19791−19798.
(71) Xiang, Z.; Zhao, J.; Yi, D.; Di, Z.; Li, L. *Angew. Chem., Int. Ed.* **2021**, *60* (42), 22659−22663.
(72) Watson, E. E.; Angerani, S.; Sabale, P. M.; Winssinger, N. *J. Am. Chem. Soc.* **2021**, *143* (12), 4467−4482.

https://doi.org/10.1021/acs.analchem.4c02622
Anal. Chem. 2024, 96, 18645−18654